PASJ: Publ. Astron. Soc. Japan **58**, 777–785, 2006 August 25

Bigradient Phase Referencing

Akihiro DOI,[1] Kenta FUJISAWA,[1] Asao HABE,[2] Mareki HONMA,[3,4] Noriyuki KAWAGUCHI,[3,4]
Hideyuki KOBAYASHI,[5,3] Yasuhiro MURATA,[6,7] Toshihiro OMODAKA,[8]
Hiroshi SUDOU,[9] and Hiroshi TAKABA[9]

[1]*Faculty of Science, Yamaguchi University, 1667-1 Yoshida, Yamaguchi, Yamaguchi 753-8512*
[2]*Division of Physics, Graduate School of Science, Hokkaido University, N10W8, Sapporo, Hokkaido 060-0810*
[3]*National Astronomical Observatory of Japan, 2-21-1 Osawa, Mitaka, Tokyo 181-8588*
[4]*Department of Astronomical Science, Graduate University for Advanced Studies, 2-21-1 Osawa, Mitaka, Tokyo 181-8588*
[5]*Mizusawa VERA Observatory, 2-12 Hoshigaoka, Mizusawa, Iwate 023-0861*
[6]*The Institute of Space and Astronautical Science, Japan Aerospace Exploration Agency, 3-1-1 Yoshinodai, Sagamihara, Kanagawa 229-8510*
[7]*Department of Space and Astronautical Science, The Graduate University for Advanced Studies, 3-1-1 Yoshinodai, Sagamihara, Kanagawa 229-8510*
[8]*Faculty of Science, Kagoshima University, 1-21-30 Korimoto, Kagoshima, Kagoshima 890-0065*
[9]*Faculty of Engineering, Gifu University, 1-1 Yanagido, Gifu, Gifu 501-1193*

(Received 2006 January 2; accepted 2006 April 26)

Abstract

We propose bigradient phase referencing (BPR), a new radio-observation technique, and report on its performance using the Japanese very-long-baseline-interferometry network (JVN). In this method, a weak source is detected by phase-referencing using a primary calibrator, in order to play a role as a secondary calibrator for phase-referencing to a weak target. We will be given the opportunity to select a calibrator from lots of milli-Jansky sources, one of which may be located at a position closer to the target. With such a smaller separation, high-quality phase-referencing can be achieved. A subsequent more-sophisticated calibration can relocate the array's focus to a hypothetical point much closer to the target; a higher quality of phase referencing is available. Our demonstrative observations with strong radio sources have proved the capabilities of the BPR in terms of the image dynamic ranges and astrometric reproducibility. The image dynamic range on a target has been improved by a factor of about six compared to that of normal phase-referencing; the resultant position difference of the target's emission between two epochs was only 62 ± 50 microarcsecond, even with less than 2300-km baselines at 8.4 GHz and fast-switching between a target–calibrator pair separated by a $2.^\circ1$.

Key words: astrometry — atmospheric effects — phase-referencing — techniques: interferometric — very-long-baseline interferometry

1. Introduction

A phase-referencing technique allows very-long-baseline interferometry (VLBI) to conduct relative astrometry with an accuracy of less than 1 milliarcsecond (mas) and to detect very weak sources at the mJy level. The quality of phase referencing is limited by residual errors in differential phases between a target and a calibrator (e.g., Beasley, Conway 1995). The most important error component is the uncertainty of atmospheric models in correlators. The differential excess-path length between two sources at different elevations is significantly harmful, even with a zenith phase-delay error of only a few centimeters and a separation of sources of only one degree (Beasley, Conway 1995; Reid et al. 1999). Possible solutions are: (1) estimating the unknown phase-delay at the zenith, (2) determining the residual phase gradient in the sky, and (3) using a calibrator very close to a target. It is advisable to apply all of these solutions simultaneously. The first solution can be achieved by geodetic-like observations (Brunthaler et al. 2005; Mioduszewski, Kogan 2004; Reid, Brunthaler 2004) or by parallel plate air modeling of the long-term phase drifts (Reid et al. 1999; Brunthaler et al. 2005). The data processing of geodetic-like observations is supported by the task DELZN of the Astronomical Image Processing System (AIPS, Greisen 2003), developed at the US National Radio Astronomy Observatory. The second solution can be achieved by using several strong calibrators over several degrees; this calibration process is also supported by the task ATMCA in the AIPS (Fomalont, Kogan 2005).

The third solution, using a calibrator very close to a target, depends on a matter of blind chance. However, it is promising if the array's sensitivity is significantly improved, since the surface number density of radio sources dramatically increases in a fainter sky (e.g., Fomalont et al. 1991). The present paper proposes a bigradient phase-referencing (BPR) method, which gives us a chance to utilize such weak radio sources as calibrators. Once a weak source very close to a very weak target is detected by phase-referencing using a strong calibrator, and then plays a role as a calibrator for phase-referencing to detect a very weak target. Such a two-step approach is responsible for its name. Furthermore, assuming that the residual phase components are linear around the target (Fomalont, Kopeikin

2003), the array's focus on the weak calibrator can relocate to a point much closer to the target. Hence, the BPR leads to be nearly free from long-term phase drifts.

In the present paper, we present the BPR method and its observational tests. In section 2 we describe the principle of the method and predict the final phase errors. In section 3 we report demonstrative VLBI observations. In section 4 we discuss the capability of this method. Finally, we summarize the method and the test observations in section 5.

2. Method

2.1. A Calibrator Arrangement and Scheduling

The BPR method schedules three sources: a target 'T', a primary calibrator 'C1', and a secondary calibrator 'C2'. C1 is bright enough to detect in half of the coherence time, typically a few minutes or less, depending on observing frequency and weather condition (Ulvestad 1999). We assume here that C2 provides correlated flux densities insufficient for fringe detection in half of the coherence time, but sufficient for detection by phase-referencing of several tens of minutes: it is ~ 10 mJy at centimeter bands for typical VLBI arrays. On the basis of a statistical discussion concerning the surface-number density of radio sources in the sky (e.g., Fomalont et al. 1991), C1 may be located relatively far from T, typically $\sim 2^\circ$ separation, while C2 can be found at a position significantly closer to T, possibly $< 0.^\circ 5$ separation. An example of source configuration is shown in figure 1.

Both T and C2 should be observed using phase-referencing because of their weakness. An example of schedule for the BPR is as follows:

$$\begin{aligned}&\ldots -\mathrm{C1}-\mathrm{C2}-\mathrm{C1}-\mathrm{C2}-\mathrm{C1}-\mathrm{C2}-\mathrm{C1}-\mathrm{C2}\\ &\quad -\mathrm{C1}-\ \mathrm{T}\ -\mathrm{C1}-\ \mathrm{T}\ -\mathrm{C1}-\ \mathrm{T}\ -\mathrm{C1}-\ \mathrm{T}\\ &\quad -\mathrm{C1}-\mathrm{C2}-\mathrm{C1}-\mathrm{C2}-\mathrm{C1}-\mathrm{C2}-\mathrm{C1}-\mathrm{C2}\\ &\quad -\mathrm{C1}-\ \mathrm{T}\ -\mathrm{C1}-\ \mathrm{T}\ -\mathrm{C1}-\ \mathrm{T}\ -\mathrm{C1}-\ \mathrm{T}\ -\ldots\end{aligned} \tag{1}$$

It consists of sets of fast-switching for two pairs: C2–C1 and T–C1. The schedule intends to remove rapid phase fluctuations by fast-switching, and to change the reference point C1 into C2 by pair-swapping in order to reduce the separation angle from T. The scans for the C2–C1 pair must be allocated every less than 1 hour, so that long-term phase drifts can be tracked. The number of iterations of fast-switching for the C2–C1 pair should be set so as to secure the detection of C2 with a signal-to-noise ratio of more than 5, for successful self-calibration in the phase domain.

2.2. Observation Equations

With such an observing schedule, an observer will obtain raw visibility data for the target and two calibrators. After determining amplitude-gain, delay, and delay-rate solutions using C1, all we have to consider are the phase terms. The observed, raw visibility phases, ϕ_{OBS}, involve various phase terms:

$$\phi^{\mathrm{C1}}_{\mathrm{OBS}} = \phi^{\mathrm{C1}}_{\mathrm{stru}} + \phi^{\mathrm{C1}}_{\mathrm{pos}} + \phi^{\mathrm{C1}}_{\mathrm{inst}} + \phi^{\mathrm{C1}}_{\mathrm{geo}} + \phi^{\mathrm{C1}}_{\mathrm{atmo}} + \phi^{\mathrm{C1}}_{\mathrm{rapid}} \tag{2}$$

$$\phi^{\mathrm{C2}}_{\mathrm{OBS}} = \phi^{\mathrm{C2}}_{\mathrm{stru}} + \phi^{\mathrm{C2}}_{\mathrm{pos}} + \phi^{\mathrm{C2}}_{\mathrm{inst}} + \phi^{\mathrm{C2}}_{\mathrm{geo}} + \phi^{\mathrm{C2}}_{\mathrm{atmo}} + \phi^{\mathrm{C2}}_{\mathrm{rapid}} \tag{3}$$

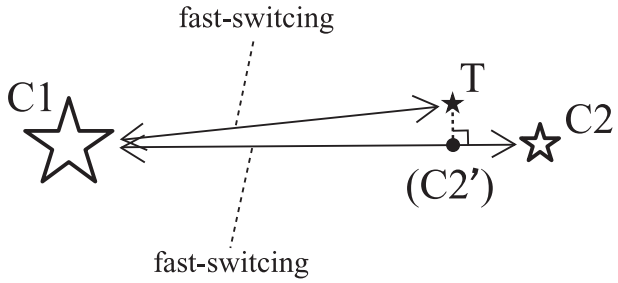

Fig. 1. Example of source configuration around a target T on the celestial sphere, and scheduling. Only a primary calibrator C1 is fringe-detectable. C2 is a secondary calibrator, a weak source. C2′ is a hypothetical calibrator, on the blank sky at the tangential point on the C1–C2 line from T.

$$\phi^{\mathrm{T}}_{\mathrm{OBS}} = \phi^{\mathrm{T}}_{\mathrm{stru}} + \phi^{\mathrm{T}}_{\mathrm{pos}} + \phi^{\mathrm{T}}_{\mathrm{inst}} + \phi^{\mathrm{T}}_{\mathrm{geo}} + \phi^{\mathrm{T}}_{\mathrm{atmo}} + \phi^{\mathrm{T}}_{\mathrm{rapid}}, \tag{4}$$

where, ϕ^{C1}, ϕ^{C2}, and ϕ^{T} are phase terms for C1, C2 and T, respectively. ϕ_{stru} is a phase term originating in the source structure; ϕ_{pos} is a positional-phase delay relative to the phase-tracking center; ϕ_{inst} is the instrumental-phase delay; ϕ_{geo} is the geometric-phase delay error; ϕ_{atmo} is the tropospheric/ionospheric-phase delay error; and ϕ_{rapid} is a rapidly variable phase due to water vapor flowing at low altitude. We ignore the thermal phase noise and the calibration errors in the present paper. We deal with the phase terms of the source position and the structure separately, in order to show an astrometric term and its error expressly in the last equation. The time scales of the change of these phase-error components are usually more than several tens of minutes, except for ϕ_{rapid}, in which the time scale is typically a few minutes or less.

2.3. Calibrations of Bigradient Phase Referencing

Data of C1 have sufficiently high signal-to-noise ratios to perform self-calibration. Hence, a sufficiently feasible source structure model can be obtained:

$$\phi^{\mathrm{C1}}_{\mathrm{OBS}} = \Phi^{\mathrm{C1}}_{\mathrm{stru}} + \Phi_{\mathrm{SN1}}, \tag{5}$$

where

$$\Phi_{\mathrm{SN1}} = \phi^{\mathrm{C1}}_{\mathrm{pos}} + \phi^{\mathrm{C1}}_{\mathrm{inst}} + \phi^{\mathrm{C1}}_{\mathrm{geo}} + \phi^{\mathrm{C1}}_{\mathrm{atmo}} + \phi^{\mathrm{C1}}_{\mathrm{rapid}}. \tag{6}$$

An antenna-based solution table, provided by the self-calibration, includes all terms other than the source structure. This is a 'solution table 1,' Φ_{SN1}. We express a determined term using its capital in the present paper.

With this solution table, we can do phase corrections to both C2 and T, so that their phases are free from rapid phase fluctuations due to water vapor. The calibration on C2 is as follows:

$$\begin{aligned}\phi^{\mathrm{C2}}_{\mathrm{OBS}} - \Phi_{\mathrm{SN1}} &= \phi^{\mathrm{C2}}_{\mathrm{stru}} + \phi^{\mathrm{C2}}_{\mathrm{pos}} + \phi^{\mathrm{C2}}_{\mathrm{inst}} + \phi^{\mathrm{C2}}_{\mathrm{geo}} + \phi^{\mathrm{C2}}_{\mathrm{atmo}} + \phi^{\mathrm{C2}}_{\mathrm{rapid}}\\ &\quad - \left(\phi^{\mathrm{C1}}_{\mathrm{pos}} + \phi^{\mathrm{C1}}_{\mathrm{inst}} + \phi^{\mathrm{C1}}_{\mathrm{geo}} + \phi^{\mathrm{C1}}_{\mathrm{atmo}} + \phi^{\mathrm{C1}}_{\mathrm{rapid}}\right)\\ &= \phi^{\mathrm{C2}}_{\mathrm{stru}} + \Delta\phi^{\mathrm{C2-C1}}_{\mathrm{pos}} + \Delta\phi^{\mathrm{C2-C1}}_{\mathrm{inst}} + \Delta\phi^{\mathrm{C2-C1}}_{\mathrm{geo}}\\ &\quad + \Delta\phi^{\mathrm{C2-C1}}_{\mathrm{atmo}} + \Delta\phi^{\mathrm{C2-C1}}_{\mathrm{rapid}},\end{aligned} \tag{7}$$

where $\Delta\phi^{\mathrm{C2-C1}}_i \equiv \phi^{\mathrm{C2}}_i - \phi^{\mathrm{C1}}_i$ are differential phase terms. Presumably, $\Delta\phi^{\mathrm{C2-C1}}_{\mathrm{rapid}} \approx 0$, because its random fluctuation is not responsible for a systematic residual, and thus should

be averaged out. Also, $\Delta\phi_{\rm inst}^{\rm C2-C1} \approx 0$, because an identical receiving system is used. The calibration on T can be done in the same manner; this is normal phase-referencing, which has been commonly used (Beasley, Conway 1995).

The other differential phase terms may not be zero. They are responsible for long-term phase drifts, which may cause some apparent position shift and a degradation of the image dynamic range. As we mentioned above, the time scales of change of these errors are usually more than several tens of minutes; we can integrate the data coherently in a period of less than their time scales. When signal-to-noise ratios sufficient to do self-calibration are available on C2 by this integration, its source structure model can be determined. Then, equation (7) becomes

$$\phi_{\rm OBS}^{\rm C2} - \Phi_{\rm SN1} \approx \Phi_{\rm stru}^{\rm C2} + \Phi_{\rm SN2}, \tag{8}$$

where

$$\Phi_{\rm SN2} \equiv \Delta\phi_{\rm pos}^{\rm C2-C1} + \Delta\phi_{\rm geo}^{\rm C2-C1} + \Delta\phi_{\rm atmo}^{\rm C2-C1}. \tag{9}$$

Thus, we obtain a 'solution table 2,' $\Phi_{\rm SN2}$. Here we assumed that the first self-calibration on C2 is done using a tentative point-source model at the phase-tracking center, in order to include $\phi_{\rm pos}^{\rm C2}$ into the solution table 2 for astrometry.

We now apply both the solution tables 1 and 2 to the target data;

$$\begin{aligned}
&\phi_{\rm OBS}^{\rm T} - (\Phi_{\rm SN1} + \Phi_{\rm SN2}) \\
&= \phi_{\rm stru}^{\rm T} + \phi_{\rm pos}^{\rm T} + \phi_{\rm inst}^{\rm T} + \phi_{\rm geo}^{\rm T} + \phi_{\rm atmo}^{\rm T} + \phi_{\rm rapid}^{\rm T} \\
&\quad - \left(\phi_{\rm pos}^{\rm C1} + \phi_{\rm inst}^{\rm C1} + \phi_{\rm geo}^{\rm C1} + \phi_{\rm atmo}^{\rm C1} + \phi_{\rm rapid}^{\rm C1}\right. \\
&\quad \left. + \Delta\phi_{\rm pos}^{\rm C2-C1} + \Delta\phi_{\rm geo}^{\rm C2-C1} + \Delta\phi_{\rm atmo}^{\rm C2-C1}\right) \\
&= \phi_{\rm stru}^{\rm T} + \Delta\phi_{\rm pos}^{\rm T-C2} + \Delta\phi_{\rm inst}^{\rm T-C1} + \Delta\phi_{\rm rapid}^{\rm T-C1} \\
&\quad + \left(\Delta\phi_{\rm geo}^{\rm T-C2} + \Delta\phi_{\rm atmo}^{\rm T-C2}\right).
\end{aligned} \tag{10}$$

This equation is very similar to equation (7), but it includes the T–C2 pair. Again, $\Delta\phi_{\rm inst}^{\rm T-C1} \approx 0$ and $\Delta\phi_{\rm rapid}^{\rm T-C1} \approx 0$. The process in this equation has replaced C1 with C2 as a reference point, where the array's focus is strictly optimized. In other words, we can make a substantially phase-referencing for the T–C2 pair without fast-switching between them. A fringe-undetectable source becomes useful as a reference calibrator. Because the separation angle of the T–C2 pair is smaller than that of the T–C1 pair, $\Delta\phi_{\rm geo}^{\rm T-C2} < \Delta\phi_{\rm geo}^{\rm T-C1}$ and $\Delta\phi_{\rm atmo}^{\rm T-C2} < \Delta\phi_{\rm atmo}^{\rm T-C1}$. This means that the differential excess path becomes smaller, and we would obtain a better image quality compared with that of the normal phase-referenced image. This is bigradient phase-referencing. An astrometric measurement of T can be done relative to C2, because of $\Delta\phi_{\rm pos}^{\rm T-C2}$, with an uncertainty of $\Delta\phi_{\rm geo}^{\rm T-C2} + \Delta\phi_{\rm atmo}^{\rm T-C2}$, as shown equation (10).

In most cases, observers have to be careful about $\phi_{\rm pos}^{\rm C2}$ in the stage of self-calibration on C2 [equations (8) and (9)]. The mas-scale position of C2 may be unknown when scheduling, because such a weak source is not cataloged into the International Celestial Reference Frame (ICRF, Ma et al. 1998). In the phase-referenced image of C2 [equation (7)], an emission peak may initially appear shifted by several tens of mas, even if the phase-tracking center was set based on a position measured with the Very Large Array (VLA) A-array configuration, etc. This leads to a too-large $\Phi_{\rm SN2}$ to make phase-connections without 2π ambiguity. Also, the requirement of position accuracy of C2 is the same as that of C1, because C2 has become a reference calibrator as a substitute for C1 in the BPR. A large position error of a reference calibrator will degrade the dynamic range of the target image (subsubsection 17.3.5 of Beasley and Conway 1995). We recommend correcting the phase-tracking center to an accurate position by post processing with the tasks CLCOR or UVFIX in the AIPS, before self-calibration on C2.

2.4. A More-Sophisticated Calibration

The solution table 2, $\Phi_{\rm SN2}$, has tracked the long-term phase drift between the C2–C1 pair, shown as equation (9). However, we hope ultimately to know at between the T–C1 pair. The method of Fomalont and Kogan (2005) achieves this using more than one calibrator around a target, based on the assumption that long-term phase variations are linear over the region of the sources (Fomalont, Kopeikin 2003). We also apply the same assumption to an additional calibration, which is more-sophisticated than the BPR. The array's focus has moved to C2 from C1 by the BPR (subsection 2.3). This means that solution table 2 has an ability to shift the focus. We can make a new focus at any point on line C2–C1, as long as the linearity is valid. In the more-sophisticated calibration, we establish a hypothetical calibrator, C2′, on the blank sky at the tangential point on the C1–C2 line from T, by scaling $\Phi_{\rm SN2}$ with a factor r, where $r \equiv (\theta^{\rm C1-C2'}/\theta^{\rm C1-C2})$, $\theta^{\rm C1-C2'}$ and $\theta^{\rm C1-C2}$ are separation angles of C1–C2′ and C1–C2, respectively (figure 1). If both the solution table 1 and this modified solution table 2 are applied to the target data,

$$\begin{aligned}
&\phi_{\rm OBS}^{\rm T} - (\Phi_{\rm SN1} + r \times \Phi_{\rm SN2}) \\
&= \phi_{\rm stru}^{\rm T} + \phi_{\rm pos}^{\rm T} + \phi_{\rm geo}^{\rm T} + \phi_{\rm atmo}^{\rm T} + \phi_{\rm inst}^{\rm T} + \phi_{\rm rapid}^{\rm T} \\
&\quad - \left[\left(\phi_{\rm pos}^{\rm C1} + \phi_{\rm geo}^{\rm C1} + \phi_{\rm atmo}^{\rm C1} + \phi_{\rm inst}^{\rm C1} + \phi_{\rm rapid}^{\rm C1}\right)\right. \\
&\quad \left. + r \times \left(\Delta\phi_{\rm pos}^{\rm C2-C1} + \Delta\phi_{\rm geo}^{\rm C2-C1} + \Delta\phi_{\rm atmo}^{\rm C2-C1}\right)\right] \\
&= \phi_{\rm stru}^{\rm T} + \Delta\phi_{\rm pos}^{\rm T-C1} - r \times \Delta\phi_{\rm pos}^{\rm C2-C1} \\
&\quad + \Delta\phi_{\rm inst}^{\rm T-C1} + \Delta\phi_{\rm rapid}^{\rm T-C1} + \left[\left(\Delta\phi_{\rm geo}^{\rm T-C1} - r \times \Delta\phi_{\rm geo}^{\rm C2-C1}\right)\right. \\
&\quad \left. + \left(\Delta\phi_{\rm atmo}^{\rm T-C1} - r \times \Delta\phi_{\rm atmo}^{\rm C2-C1}\right)\right].
\end{aligned} \tag{11}$$

Again, $\Delta\phi_{\rm inst}^{\rm T-C1} \approx 0$ and $\Delta\phi_{\rm rapid}^{\rm T-C1} \approx 0$. Because of the linearity, the terms $r \times \Delta\phi_{\rm geo}^{\rm C2-C1}$ and $r \times \Delta\phi_{\rm atmo}^{\rm C2-C1}$ virtually correspond to differential geometric and atmospheric phase-delays between C2′ and C1: $r \times \Delta\phi_{\rm geo}^{\rm C2-C1} = \Delta\phi_{\rm geo}^{\rm C2'-C1}$ and $r \times \Delta\phi_{\rm atmo}^{\rm C2-C1} = \Delta\phi_{\rm atmo}^{\rm C2'-C1}$. Finally, equation (11) becomes

$$\begin{aligned}
&\phi_{\rm OBS}^{\rm T} - (\Phi_{\rm SN1} + r \times \Phi_{\rm SN2}) \\
&\approx \phi_{\rm stru}^{\rm T} + \Delta\phi_{\rm pos}^{\rm T-C1} - r \times \Delta\phi_{\rm pos}^{\rm C2-C1} + \left(\Delta\phi_{\rm geo}^{\rm T-C2'} + \Delta\phi_{\rm atmo}^{\rm T-C2'}\right).
\end{aligned} \tag{12}$$

This is substantially a phase-referencing for the T–C2′ pair, although there is no fast-switching between them. The modified phase solutions of self-calibration have made the

array's focus on the sky toward C2′, much closer to the target.

The astrometric term in equation (12) is $\Delta\phi_{\rm pos}^{\rm T-C1}$. Because the term $r \times \Delta\phi_{\rm pos}^{\rm C2-C1}$ consists of only positional terms, it makes only a slight position shift without degrading the image dynamic range. Even with ICRF calibrators, their absolute-position uncertainties (~ 0.3 mas, Ma et al. 1998; Fey et al. 2004) may be responsible for the term. Since the differences between the real positions and phase-tracking centers are unpredictable, $r \times \Delta\phi_{\rm pos}^{\rm C2-C1}$ is also unpredictable. However, this will practically not contribute to astrometric errors in observations of relative astrometry, because $r \times \Delta\phi_{\rm pos}^{\rm C2-C1}$ is duplicated every epoch if the relative positions between the emission peaks of calibrators and the phase-tracking centers are not changed during any epoch. Thus, we can conduct relative astrometry for measuring the proper motion during a series of monitoring observations. Please note that the observer must use identical phase-tracking centers every epoch, and the first self-calibrations using the structure models at the phase-tracking centers.

The terms of ($\Delta\phi_{\rm geo}^{\rm T-C2'} + \Delta\phi_{\rm atmo}^{\rm T-C2'}$) are expected to be zero, if the position of C2′ is coincident with that of T, i.e., all of the three sources align exactly on a straight line. If the sources are misaligned, these terms become a phase error, depending on the separation angle between C2′ and T. Because the BPR makes a lot of weaker calibrators usable, observers will have a desirable allocation of sources in the sky much more easily. Possible solutions to reduce this remaining error of the misaligned case are discussed in subsection 4.3.

2.5. Calibration Errors

In addition to the errors theoretically expected in the method, there are various calibration errors. These kinds of errors are usually not so large compared to the long-term phase drifts, but still sufficient to affect the quality of a phase-referenced image. Observers must be careful to address them as much as possible, when pursuing accurate astrometry.

(1) The purity of the solution tables is related to the quality of self-calibration in equations (5) and (8). Very complex source structures or low signal-to-noise ratios make it difficult to separate $\Phi_{\rm stru}$ from the other phase terms. This calibration error would be significant, because the BPR involves self-calibration twice, and because one of two calibrators is always a weak source. An antenna-based phase solution with a signal-to-noise ratio of 3 corresponds to an accuracy of $\sim 21^\circ$ theoretically (Thompson et al. 2001), which would be as large as systematic phase components to be corrected. Hence, we recommend the use of C2 with an signal-to-noise ratio of more than 5. Note that phase signals are usually weaker on longer baselines.

(2) Rapid phase fluctuations with the same as, or less than, period of fast-switching cannot be removed, although we assumed $\Delta\phi_{\rm rapid}^{\rm C2-C1} \approx 0$ and $\Delta\phi_{\rm rapid}^{\rm T-C1} \approx 0$. The remaining fluctuations tend to be random and averaged out, but are responsible for the coherence loss. This situation also arises in normal phase-referencing of fast-switching. A dual-beam observation, as the VERA, is presumably the most effective way against such a random-phase fluctuation.

(3) The longer term changes of $\phi_{\rm pos}$, $\phi_{\rm atmo}$, and $\phi_{\rm geo}$ have time scales of more than several tens of minutes. The pair-swapping tracks them, but cannot monitor their fluctuations with shorter time scales due to the absence of fast switching between T and C2. The fluctuations affect not only phase measurements in C2 scans, but also for calibration parameters that will be made for T by interpolation between the C2 scans. We recommend that the pair-swapping period is about 20 minutes, which provides some redundancy in the time scale of long-term phase drifts, when accurate astrometry is required. The fluctuations will be averaged out, although some coherence loss is not avoidable.

(4) The structure change of calibrators results in a position shift of the target; astrometric errors of 100 microarcseconds over observations longer than several months are possible. Although this is not a kind of calibration error, it is not avoidable for observers. The intrinsic position change on a calibrator will bring the same position shift on the target without degrading its image dynamic range. It is necessary to use calibrators with stable structures, preferably point sources; do not use super-luminul quasars even if high signal-to-noise ratios are expected.

3. Test Observations

We present demonstrative VLBI observations by the BPR method in this section. Although this method aims to detect a weak target using a weak calibrator and a strong calibrator, for easy inspection of visibility-phase correction, here we selected a target and two calibrators from strong ICRF radio sources, as follows:

- 3C 345 as a target 'T',
- NRAO 512 as a secondary calibrator 'C2',
- DA 426 as a primary calibrator 'C1.'

The relative locations of these sources are similar to figure 1, but align more straightly on an east–west direction on the celestial sphere. C1 and T, a primary pair, are separated by $2.^\circ09$; C1 and C2, a secondary pair, are separated by $2.^\circ57$; C2 and T are separated by $0.^\circ48$. T and C2′ are separated by only $2.'1$.

3.1. Observations

VLBI imaging observations with the BPR method were carried out at two epochs with the Japanese VLBI network (JVN), a newly-established VLBI network with $\sim$ 50–2300 km baselines across the Japanese islands (K. Fujisawa et al. in preparation). This array consists of ten antennas, including four radio telescopes of the VLBI Exploration of Radio Astrometry project (VERA, Kobayashi et al. 2003). The telescope participants for the observations are listed in table 1. Right-circular polarization was received in the X-band. Two frequency bands, 8400–8416 MHz (IF1) and 8432–8448 MHz (IF2), were selected. The VSOP-terminal system was used as a digital back-end; digitized data in 2-bit quantization were recorded onto magnetic tapes at a data rate of 128 Mbps. Correlation processing was performed with the Mitaka FX correlator (Shibata et al. 1998) at the National Astronomical Observatory of Japan.

The switching-cycle period of phase-referencing was 5 minutes. A set of switching cycles for the primary pair (T–C1) took about 20 minutes; a set for the secondary pair

Table 1. Array configurations for our observations.

Epoch	Date	Telescopes
1st	2005 Sep 25 08:00–12:30 UT	VERA ×4 (Mizusawa 20 m, Ogasawara 20 m, Iriki 20 m, Ishigaki 20 m)
2nd	2005 Oct 23 06:00–12:00 UT	VERA ×4 (Kashima 34 m, Tsukuba 32 m, Usuda 64 m, Yamaguchi 32 m)

Table 2. Phase-referencing qualities in images of 3C 345.*

Epoch	Antenna	Method	$I^{\rm p}$ (Jy beam^{-1})	$\sigma_{\rm img}$ (mJy beam^{-1})	$I^{\rm p}/\sigma_{\rm img}$	σ_ϕ (deg)	$\Delta\alpha$ (mas)	$\Delta\delta$ (mas)
(1)	(2)	(3)	(4)	(5)	(6)	(7)	(8)	(9)
1st	VERA	PR	3.49	291	12	65	-1.103 ± 0.118	$+0.925 \pm 0.059$
		BPR	4.03	107	37	26	-0.956 ± 0.054	$+0.238 \pm 0.025$
		BPR + α	4.06	97.4	41	30	-0.999 ± 0.050	$+0.374 \pm 0.023$
		self-cal.	4.32	9.23	468	21	...	...
2nd	VERA	PR	3.62	290	12	69	-1.308 ± 0.159	$+1.198 \pm 0.074$
		BPR	3.90	88.7	44	21	-0.725 ± 0.044	$+0.077 \pm 0.022$
		BPR + α	3.93	100	39	28	-0.871 ± 0.050	$+0.307 \pm 0.025$
		self-cal.	4.10	15.8	259	19	...	...
	all	PR	3.04	400	8	79	-0.926 ± 0.313	$+1.243 \pm 0.175$
		BPR	4.34	144	30	33	-1.001 ± 0.083	$+0.126 \pm 0.043$
		BPR + α	4.56	93.2	49	30	-0.967 ± 0.055	$+0.320 \pm 0.028$
		self-cal.	4.91	7.26	676	18	...	...

* (1) Observing epoch, (2) antennas used for mapping, (3) calibration method. 'PR' represents normal phase referencing. 'BPR' represents bigradient phase referencing. 'BPR + α' represents more-sophisticated calibration. 'Self-cal.' represents self-calibration. (4) Peak intensity, (5) RMS of image noise, (6) image dynamic range, (7) RMS of visibility–phase scatter, (8) and (9) position shifts from phase-tracking center of 3C 345. These were measured by two-dimensional Gaussian fitting using task JMFIT of AIPS.

(C2–C1) also spent about 20 minutes. The two sets were scheduled alternately, as mentioned in subsection 2.1. Thus, the pair-swapping cycle period was about 40 minutes.

3.2. Data Reduction

Data reduction procedures were performed for three data sets: 1st-epoch data (VERA antennas), 2nd-epoch data from only the VERA antennas, and 2nd-epoch data from all the antennas. The correlated data were reduced using the AIPS. After the initial data inspection and flagging, fringe-fitting was performed to 3C 345 and NRAO 512. Note that in this stage we did not intend to use the two sources as T or C2, but for bandpass calibration and amplitude-gain calibration, respectively. Since NRAO 512 is the most ideal point source up to our longest baseline ($\sim 50\,{\rm M}\lambda$), self-calibration in terms of the amplitude provided us with solutions of amplitude–gain variation relative to each antenna with an accuracy of about 1%. We conducted absolute-amplitude scaling using NRAO 512 with 0.89 ± 0.09 Jy, a single-dish measurement with the Yamaguchi 32-m radio telescope (Fujisawa et al. 2002) at 8.38 GHz on 2005 November 12. After these processes, we deleted the solutions of fringe-fitting for 3C 345 and NRAO 512. Data obtained at elevations of less than $\sim 25^\circ$ were flagged out. We utilized no a-priori gain parameter in both the amplitude and the phase, except for the absolute flux scaling.

Next, we performed fringe-fitting for C1 (DA 426), then established its source structure model in the Difmap software (Shepherd 1997) using deconvolution and self-calibration algorithms iteratively. With the CALIB task in the AIPS, the phase solution of self-calibration was obtained using the source structure model: we obtained a 'solution table 1' (subsection 2.3). We applied this table to the data of both T and C2. At this stage, we can obtain normal phase-referenced images.

The phase-referenced visibilities of C2 (NRAO 512) were coherent for at least several tens of minutes (described in subsubsection 3.3.2), as we had assumed. C2 was supposed to have sufficient signal-to-noise ratios to perform self-calibration in phase when integrated for several tens of minutes, even if when down to ~ 10 mJy. We successfully obtained a 'solution table 2' by self-calibration for NRAO 512 in a solution interval of 40 minutes. Target images, which were synthesized from visibilities corrected with both calibration tables 1 and 2, are shown in figure 2b, f, and j; these are images provided by the BPR method.

The three sources quasi-perfectly align on the sky. This is an ideal situation for a more sophisticated calibration (subsubsection 2.4). The phase solutions in solution table 2 was scaled down to r [$= (\theta^{\rm C1-C2'}/\theta^{\rm C1-C2})$] times, and then the modified solution table was applied to the target data together with solution table 1. The resultant images are shown in figure 2c, g, and k. For a comparison, images corrected by self-calibration both in amplitude and phase are also shown in figure 2d, h, and l.

The number of usable visibilities in the data set of 2nd-epoch from only the VERA antennas were $\sim 30\%$ less than the 1st-epoch ones, because a significant fraction of C1's scans

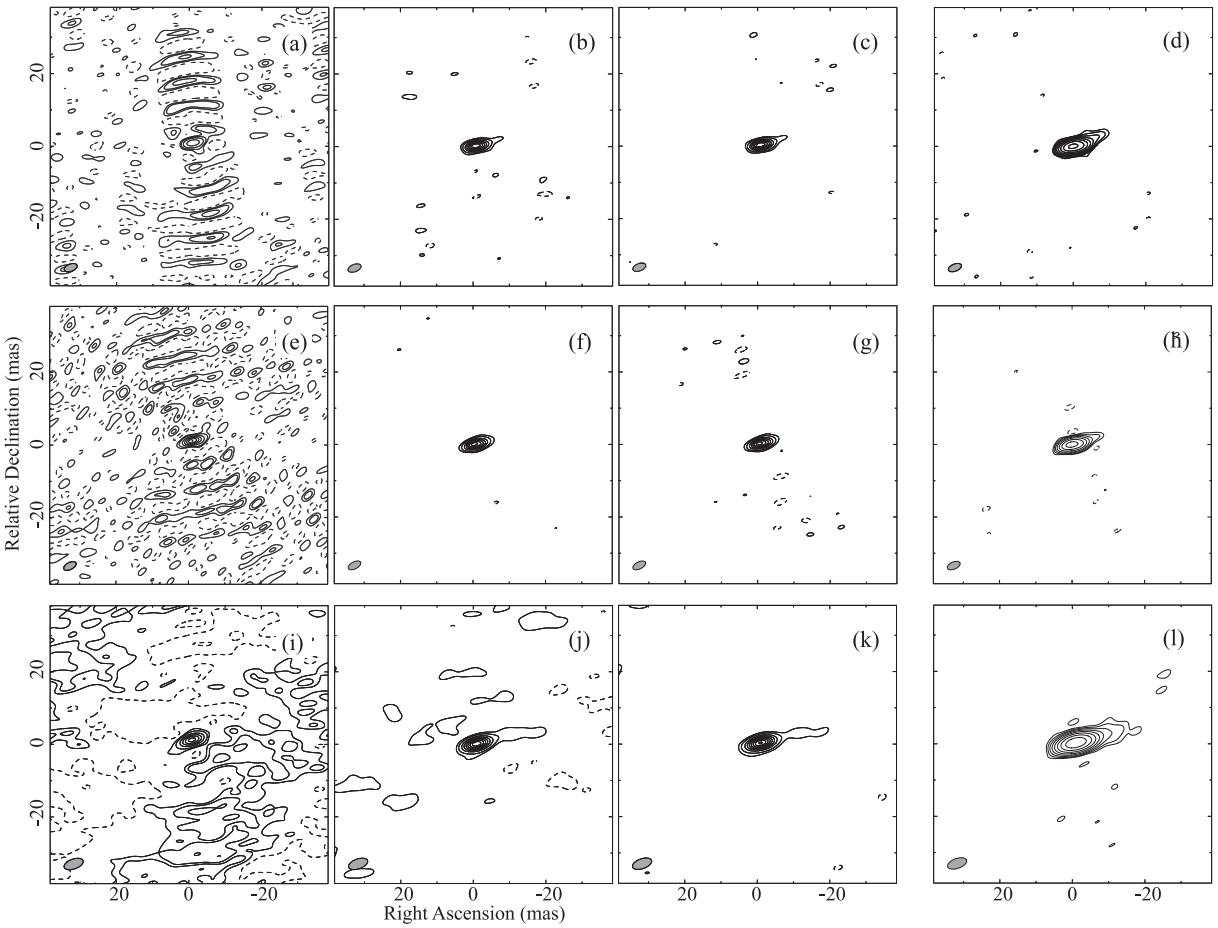

Fig. 2. Contour maps of target 3C 345. (upper panels) Images at the first epoch with four telescopes of the VERA. (a) Normal phase-referenced image. (b) Bigradient phase-referenced image. (c) Image made by more-sophisticated calibration. Contours of (a)–(c) start from $3\sigma_c$, where σ_c is RMS of image noise on the image (c) (see table 2). (d) Self-calibrated image. Contours of (d) start from $3\sigma_d$, where σ_d is RMS of image noise on the image (d). Synthesized beams, shown at the lower-left of each image, are of 3.75 mas × 2.02 mas at a position angle of $-69.^\circ3$. (middle panels) Images at the second epoch with only four telescopes of the VERA. (e) Normal phase-referenced image. (f) Bigradient phase-referenced image. (g) Image made by more-sophisticated calibration. Contours of (e)–(g) start from $3\sigma_g$. (h) Self-calibrated image. Contours of (h) start from $3\sigma_h$. Synthesized beams are of 2.00 mas × 3.52 mas at a position angle of $-67.^\circ3$. (lower panels) Images at the second epoch with all telescopes. (i) Normal phase-referenced image. (j) Bigradient phase-referenced image. (k) Image made by more-sophisticated calibration. Contours of (i)–(k) start from $3\sigma_k$. (l) Self-calibrated image. Contours of (l) start from $3\sigma_l$. Synthesized beams are of 2.72 mas × 5.54 mas at a position angle of $-70.^\circ6$. Contour levels for phase-referenced images are $3\sigma \times (-1, 1, 2, 4, 6, 8, 10, 12, 14, 16)$; for self-calibrated images are $3\sigma \times (-1, 1, 2, 4, 8, 16, 32, 64, 128, 256)$. Negative contours are described in dashed-curves.

were flagged out in fringe-fitting. With such a small number of visibilities and a poor UV-coverage, the resultant images could not bear any comparison with the other data sets.

3.3. Results

3.3.1. Image quality

The images by the BPR appearing in figure 2 are dramatically improved compared to those by normal phase-referencing; the image dynamic ranges have increased by about 3.1–3.8 times (table 2). The jet structure of 3C 345 is seen in the improved images. This is the fruit of using a closer calibrator adopted in the BPR. Normal phase-referencing was from the T–C1 pair, separated by $2.^\circ09$, while the BPR was practically from the T–C2 pair, separated by only $0.^\circ48$, a 4.3-times smaller separation. Better images have been obtained by more-sophisticated calibration. This is the fruit of optimizing solution table 2 for the sky point of C2′, separated from T by only $2.'1$, a 61-times smaller separation than that of T–C1. In the VERA image at the 2nd epoch, the more-sophisticated calibration appears not to work well in terms of the image-noise level. Because of the small number of effective visibility, measurements for this data set might be somewhat inadequate.

3.3.2. Long-term phase drifts

In the BPR method, phase-referenced visibilities of C2 are supposed to be coherent for at least several tens of minutes. Additionally, more-sophisticated calibration expects that the phase of phase-referenced C2 is a linear extrapolation of the phase-drift between T and C1. We show an example of the phase-referenced visibility phases both of 3C 345 (T) and NRAO 512 (C2) in figure 3. A long-term phase-drift is seen. The phase-drift of 3C 345 was undesirable for normal phase-referencing. From DA 426's (C1's) point of view, both the two sources are at about the same direction and separation.

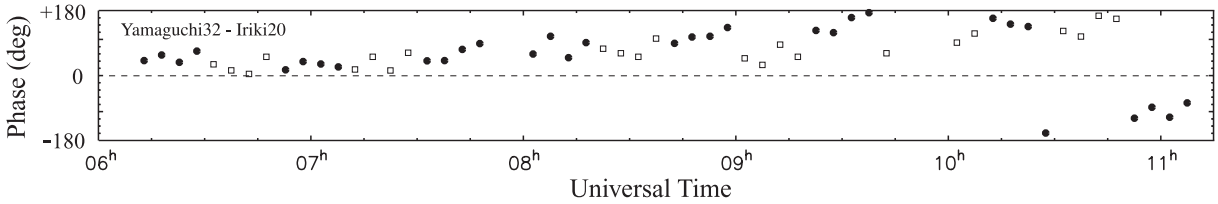

Fig. 3. Plot of the visibility phases phase-referenced by primary calibrator DA 426 on the Yamaguchi 32 m–Iriki 20 m baseline. The open squares and filled circles represent phases of 3C 345 and NRAO 512, respectively. The visibilities were averaged for 5 minutes in this plot.

The phases of NRAO 512 are supposed to be similar to the drift of 3C 345, and this expectation met the observation. Consequently, we can remove a large part of the phase drift on 3C 345 by shifting the array's focus to NRAO 512.

The phase drift of NRAO 512 became larger than that of 3C 345, especially later than $09^{\rm h}$, where elevations of these sources became lower. This deviation occurred because that the separation angle of NRAO 512–DA 426 was larger than that of 3C 345–DA 426. Consequently, the data of 3C 345 will be over-corrected by the solution table 2 in the BPR. The more-sophisticated calibration aims to correct such a difference by optimizing the solution table 2 toward the hypothetical calibrator C2′. The RMS of calibrated phases are listed in column (7) of table 2. Steady improvements were seen in the images of the 2nd epoch data from all the antennas. However, slight increases of RMS were seen in the VERA data. It may be a coincidental effect of the intrinsic structure of 3C 345; the VERA array is sensitive to the source structure because of its longest baselines in the JVN array. The improvements of the other parameters (e.g., peak intensity) are the proof of efficacy of the more-sophisticated calibration.

3.3.3. Position shifts

We evaluate here an astrometric capability from positional reproducibility between the two epochs. Because of only one month, the intrinsic changes of the source structures were presumably negligible. The measured position offsets from the phase-tracking center on the target images are listed in columns (8) and (9) of table 2. The improvements of the positional reproducibility by the BPR and more-sophisticated calibration are visualized in figure 4. The position differences between the 1st epoch and 2nd epoch of the target with all of the available antennas were steadily reduced in our calibration steps: $360 \pm 240\,\mu$as between the normal phase-referenced images, $120 \pm 57\,\mu$as between the BPR images, and finally, $62 \pm 50\,\mu$as between the images by more-sophisticated calibration. Globally, the emission peak of 3C 345 appeared at ~ 1 mas northwest from the phase-tracking center. These global position shifts include several origins, which are discussed in subsection 4.2.

4. Discussions

4.1. Phase-Referencing Capabilities

The BPR substantially achieves phase-referencing between the C2–T pair without fast-switching between them. In our tests, 3C 345 and NRAO 512 were separated by $0.^\circ48$, 4.3-times smaller than the separation angle of actual fast-switching between 3C 345 and DA 426. A long-term phase drift from atmospheric/geometric errors, therefore, was expected to be 4.3-times smaller (Beasley, Conway 1995). However, resultant dynamic ranges of BPR images have been improved only 3.1–3.8 times better than those of normal phase-referenced images. This discrepancy was probably caused by several calibration errors (subsection 2.5). The phase drifts seem to have been successfully tracked with the sampling of C2 every 40 minutes. However, this sampling frequency might be risky at some level; as can be seen in figure 3, the phases of NRAO 512 and 3C 345 are systematically different at about $9.^{\rm h}2$ UT. It is advisable to pair-switch about every 20 minutes, or to apply another observing schedule with more frequent C2 scans, such as $-$C1–C2–C1–T $-$ C1–C2–C1–T $-$ C1–…. The observation case of indeed very weak C2, which is originally supposed in the BPR, will be reported in a future paper. The BPR would give a better quality than that of the normal phase-referencing, even with a weak (~ 10 mJy) C2 with a signal-to-noise ratio of 5 in several scans using typical arrays at centimeter bands.

We briefly discuss the over-correction of the solution table 2 in the BPR method, by comparing 2nd-epoch images with all of the antennas. In the normal phase-referenced images, both of 3C 345 and NRAO 512 (not shown), very similar patterns of distorted contours are seen: positive and negative contours reside mainly at the lower-right and upper-left side corners in the images, respectively in figure 2i. On the other hand, an opposite trend appears in the contours of the BPR image of 3C 345 in figure 2j. This is an effect of an over-correction of solution table 2, which was designed for $2.^\circ57$ separation of the C1–C2 pair, rather than $2.^\circ09$ separation of the C1–T pair. The distortion trend almost disappears in the image by more-sophisticated calibration using the optimized table in figure 2k.

4.2. Astrometric Capabilities

The BPR and the more-sophisticated calibration support relative astrometry, if observers use identical phase-tracking centers every epochs (section 2). The consistency of the measured positions between our two epochs (subsubsection 3.3.3) indicated that the relative astrometry presumably worked well. The position differences among the epochs are consistent with the phase noises (table 2).

Dramatic revisions of the target position are seen particularly in declination (figure 4). This indicates that the long-term phase drifts were responsible for a large part of the declination offsets. Geometric errors should be small in the VERA's four telescopes, Kashima 34 m, and Tsukuba 32 m, whose coordinates are strictly maintained by geodetic observations. The correlator model in the Mitaka FX correlator seems to have

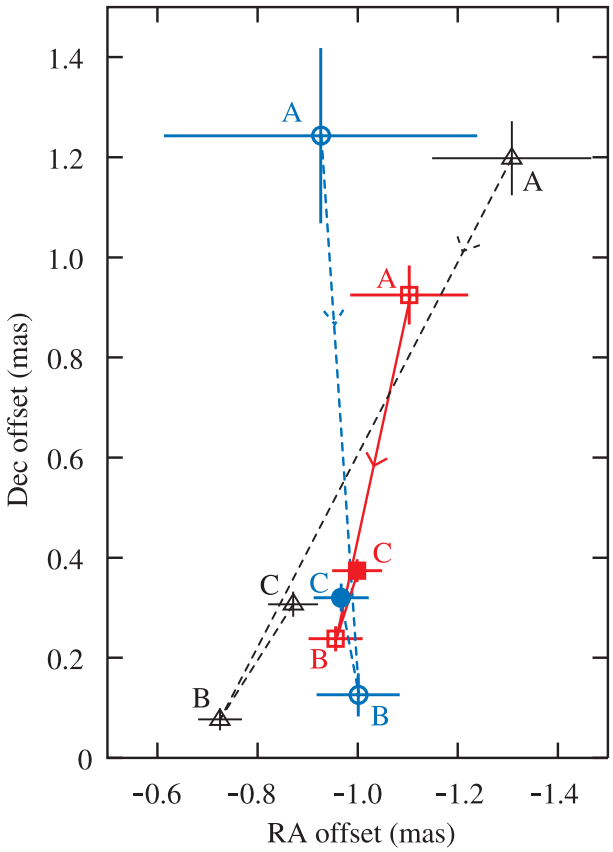

Fig. 4. Improvements in the reproducibility of the target's (3C 345) position. The origin (0, 0) of this plot is the phase-tracking center of the target. Labels A, B, and C show three different methods to measure positions. A, normal phase-referencing; B, BPR; C, more-sophisticated calibration. Three different symbols show different epochs and arrays. The squares represent the 1st-epoch measurements with the VERA antennas. The triangles represent 2nd-epoch measurements with VERA antennas. Circles represent 2nd-epoch measurements with all antennas. The most calibrated images show a position difference of only $62 \pm 50\,\mu$as between two epochs (filled symbols).

somewhat prediction errors in zenith excess-path lengths at troposphere and/or ionosphere. Note that a priori calibration for such atmospheric errors is usually performed in the VERA project.

There remain significant offsets ~ 1 mas west and $\sim 300\,\mu$as north in both the epochs, even with the more-sophisticated calibration. Since such large global offsets could not be caused by any atmospheric/geometric errors, in principle, an accumulation of intrinsic differences between actual emission's positions and phase-tracking centers of the target and two calibrators should be mainly responsible for the global offsets. This kind of offset cannot be avoided, even with the ICRF radio sources and their cataloged positions, which have uncertainties of ~ 0.3 mas (Ma et al. 1998; Fey et al. 2004), not only in the BPR and the more-sophisticated calibration but also in the normal phase-referencing. DA 426 (C1) has mas-scale jets east-southeast; 3C 345 (T) has mas-scale jets west-northwest. Hence, the global offsets pointing toward west-northwest may be reasonable.

A position difference of $62 \pm 50\,\mu$as between the two epochs in the images by more-sophisticated calibration might originate in the slightly misaligned allocation of the three sources. Strictly, the optimized solution table 2 reacted to the sky position of C2′. This position was separated by 2.′1 from T. The atmospheric and geometric errors from this separation could cause a 10–20 μas difference between the two epochs. If the three sources are perfectly aligned, the apparent positions of two epochs might coincide with each other within an error bar.

4.3. *Implications of the Methods*

Although both the BPR and the more-sophisticated calibration aim to retaliate against long-term phase drifts by reducing the separation angle, they are based on slightly different tactics. The BPR makes a weak source play a role of calibrator C2. Since self-calibration is done on C2, the array's focus shifts to C2, closer to T than C1. The more-sophisticated calibration estimates the solution of self-calibration on a hypothetical calibrator C2′ from the solution on C2. Array's focus finally shifts to C2′, closer to T than C2.

The key of the BPR is the presence of a suitable C2 at a position of less half the distance to T than that to C1. Without such a suitable C2, a BPR image will be worse than that of normal phase referencing. However, even a distant C2 may help the more-sophisticated calibration, if the sources align straightly.

The key to the more-sophisticated calibration is the linearity of the phases $\Delta\phi_{\rm atmo}$, $\Delta\phi_{\rm geo}$, and $\Delta\phi_{\rm pos}$. The linearity around sources have already been assumed in the method of ATMCA (Fomalont, Kogan 2005), which uses strong calibrators around a target to determine the phase gradient. The best performance can be obtained by both the more-sophisticated calibration and the ATMCA when sources align straightly. Even in the case of misaligned source allocation, the calibration of ATMCA can be done by estimating a two-dimensional phase gradient using three or more calibrators. Because of the same assumption, the more-sophisticated calibration also can do it. Array's focus can be established exactly at T, when $\overrightarrow{C_1C_2'} + \overrightarrow{C_1C_3'}$, i.e. $r_{12}\overrightarrow{C_1C_2} + r_{13}\overrightarrow{C_1C_3}$, $= \overrightarrow{C_1T}$. Such a calibration table is derived from the two solution tables produced by self-calibrations on C2 and C3, in addition to that on C1. Not only bright calibrators, but also weak ones, are usable as secondary calibrators, if the BPR is applied before the more-sophisticated calibration or the ATMCA. Alternatively, with only one secondary calibrator, a good calibration can be achieved if assuming that the phase gradient is in the elevation direction, because the residual phase error is mostly of tropospheric origin. This is supported by an option of the ATMCA. In such a process, observers should separate $\Delta\phi_{\rm atmo}$ from the other terms that would interact with the determination of the phase gradient. Fomalont and Kogan (2005) recommend observing for more than 3 hours to find the true positions of calibrators, in order to make $\Delta\phi_{\rm pos} \approx 0$. The term $\Delta\phi_{\rm geo}$, however, would be harmful in arrays with poorly position-determined spacecraft and/or antennas.

The BPR can make very weak sources available as calibrators. In normal phase-referencing a signal-to-noise ratio of more than ~ 5 in half of a fast-switching period is required

to obtain phase, delay, delay-rate solutions, while in the BPR a signal-to-noise ratio of ~ 5 to obtain only a phase solution in about a quarter of a pair-swapping period is acceptable. This means that we can actually use calibrators more than a few times weaker than conventional calibrators. Consequently, the BPR brings many benefits, for example: (1) observers will be given more opportunities to make phase-referencing successfully at short centimeter and millimeter bands ($\sim$ 22–86 GHz), where targets normally have little chance of being accompanied by bright calibrators with a small separation angle. (2) Phase-referencing is available even to poorly sensitive or poorly position-determined antennas, such as a space-VLBI. (3) Astrometry can be made between two weak sources, one of which has been self-calibrated. (4) Observers can easily obtain idealized calibrator arrangements on the sky plane for the subsequent more-sophisticated calibration or the ATMCA, because of much larger surface number density in the faint-source sky.

Practically, prior phase-referencing observations will be needed to find suitable calibrators around the target. We suggest that candidates are selected from flat-spectrum sources in the catalogs of the FIRST survey and so on, like the approach of 'a VLBA survey of flat-spectrum FIRST sources (Ulvestad et al. 1999).'

The BPR and the subsequent more-sophisticated calibration are universal-designed. There is no requirement of upgrades for hardware or software. All that observers have to do is the scheduling of fast-switching with less frequent pair-swapping, and data reduction with bigradient calibration processes, which can be done only with the AIPS and editing solution tables. Even with antennas whose positions have not been well-determined, or even with a correlator without precise atmospheric models, very weak targets can be detected because of a much smaller separation from C2 or C2′ than that from C1. A priori calibration by geodetic-like observations (e.g., Mioduszewski, Kogan 2004) should bring independent improvements. Therefore, the combination of such prior calibrations and our method should achieve extremely high-quality phase-referencing.

5. Summaries

The bigradient phase referencing (BPR) allows us to utilize weak calibrators, one of which may be located at a position much closer to a target. The subsequent, more-sophisticated calibration makes the array's focus to shift to a hypothetical point much closer to a target. Thanks to the much smaller separation angle, the phase-referencing quality of a target image will be dramatically improved. We described the theory of the method and expected errors. For relative astrometry, the observer must use identical phase-tracking centers every epoch, and the first self-calibrations on the calibrators using the structure models at the phase-tracking centers. Our demonstrative observation tests with strong sources (3C 345, NRAO 512, and DA 426) have shown its capabilities. Image dynamic ranges have been dramatically improved by a factor of about six, compared to normal phase-referencing. The astrometric reproducibility is $62 \pm 50\,\mu$as between our two epochs in the most calibrated cases. The observation case of a weak calibrator, which is originally supposed in the BPR, will be reported in a future paper.

The authors wish to thank the JVN team for observing assistance and support. We thank an anonymous referee for excellent suggestions and thoughtful comments. The JVN project is led by the National Astronomical Observatory of Japan (NAOJ) that is a branch of the National Institutes of Natural Sciences (NINS), Hokkaido University, Gifu University, Yamaguchi University, and Kagoshima University, in cooperation with Geographical Survey Institute (GSI), the Japan Aerospace Exploration Agency (JAXA), and the National Institute of Information and Communications Technology (NICT).

References

Beasley, A. J., & Conway, J. E. 1995, in ASP Conf. Ser. 82, Very Long Baseline Interferometry and the VLBA, ed. J. A. Zensus, P. J. Diamond, & P. J. Napier (San Fransisco: APS), 328
Brunthaler, A., Reid, M. J., & Falcke, H. 2005, APS Conf. Ser., 340, 455
Fey, A. L., et al. 2004, AJ, 127, 3587
Fomalont, E., & Kogan, L. 2005, AIPS Memo, No. 111
Fomalont, E. B., & Kopeikin, S. M. 2003, ApJ, 598, 704
Fomalont, E. B., Windhorst, R. A., Kristian, J. A., & Kellerman, K. I. 1991, AJ, 102, 1258
Fujisawa, K., Mashiyama, H., Shimoikura, T., & Kawaguchi, N. 2002, in Proc. 8th Asian-Pacific Regional Meeting, II, (Tokyo: ASJ), 3
Greisen, E. W. 2003, in Information Handling in Astronomy — Historical Vistas, ed. A. Heck (Dordrecht: Kluwer), 109
Kobayashi, H., et al. 2003, ASP Conf. Ser., 306, 367
Ma, C., et al. 1998, AJ, 116, 516
Mioduszewski, A. J., & Kogan, L. 2004, AIPS Memo, No. 110
Reid, M. J., & Brunthaler, A. 2004, ApJ, 616, 872
Reid, M. J., Readhead, A. C. S., Vermeulen, R. C., & Treuhaft, R. N. 1999, ApJ, 524, 816
Shepherd, M. C. 1997, ASP Conf. Ser., 125, 77
Shibata, K. M., Kameno, S., Inoue, M., & Kobayashi, H. 1998, in ASP Conf. Ser. 144: IAU Colloq. 164: Radio Emission from Galactic and Extragalactic Compact Sources (San Fransisco: APS), 413
Thompson, A. R., Moran, J. M., & Swenson, G. W., Jr. 2001, Interferometry and Synthesis in Radio Astronomy, 2nd ed. (New York: Wiley), 316
Ulvestad, J. S. 1999, VLBA Scientific Memo, No. 20
Ulvestad, J. S., Fomalont, E. B., & Kimora, H. 1999, BAAS, 31, 900